

Interfacial Charge Transfer between Phenyl-Capped Aniline Tetramer Films and Iron Oxide Surfaces

Amirmasoud Mohtasebi,[†] Tanzina Chowdhury,[†] Leo H. H. Hsu,[‡] Mark C. Biesinger,[§] and Peter Kruse^{*,†,‡}

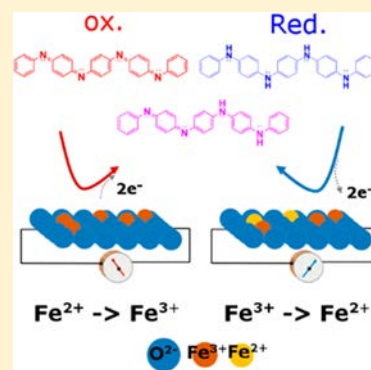
[†]Department of Chemistry and Chemical Biology, McMaster University, 1280 Main Street West, Hamilton, Ontario L8S 4M1, Canada

[‡]Department of Mechanical Engineering, McMaster University, Hamilton L8S 4L8, Canada

[§]Surface Science Western, Room LL31, 999 Collip Circle, London, Ontario N6G 0J3, Canada

S Supporting Information

ABSTRACT: Redox-active organic compounds have been studied as corrosion inhibitors for steel. Even though it is clear that chemical interactions at the organic–metal oxide interface are behind this inhibitive process, the detailed mechanism is not yet fully understood. Using phenyl-capped aniline tetramer (PCAT), we have elucidated the interactions at the interface with iron oxide. We demonstrate the partial reduction of fully oxidized PCAT and the partial oxidation of fully reduced PCAT upon interaction with iron oxide. X-ray photoelectron spectroscopy reveals the appearance of charged nitrogen structures in PCAT deposited on hematite. Iron oxide films in contact with reduced PCAT show a higher conductance due to the introduction of defects, resulting in n-doping. In contrast, the iron oxide film in contact with oxidized PCAT shows a lower conductance, indicating that defects in the film are removed via oxidation, thus reducing the doping level. This is consistent with accepted models for corrosion inhibition, in which PCAT assists in the formation of a passive oxide film. These results are indicative of interfacial charge transfer between PCAT and iron oxide. The extent of the charge transfer and the direction of redox processes depend on the oxidation state of the molecules, enabling the construction of redox-active devices, including sensors and switches.



INTRODUCTION

Redox-active organic compounds are known to protect transition metals against corrosion.¹ Their weak performance under practical corrosion conditions has prevented their widespread use in commercial settings. Therefore, a better understanding of the chemical and electronic interactions at the interface between metal oxides and redox-active organic molecules is crucial to the design of better organic corrosion inhibitor coatings. Furthermore, transition metal oxide–organic interfaces have important applications in organic electronic devices, such as photovoltaics,² light-emitting diodes,³ and thin-film transistors.⁴ All of these devices function on the basis of the charge transfer at the interface between a metal oxide and an organic layer. Metal oxides can be used in conjunction with a broad range of organic materials because their chemical and electronic properties can be tuned in order to create a desirable alignment with the energy levels of the organic layer.⁵

It was discovered in 1985 that polyaniline (PANI) electrodeposited on steel can inhibit corrosion.⁶ PANI acts as more than a simple barrier coating in this case as it was shown that breaching the organic layer does not necessarily initiate corrosion in steel presumably as a result of an electrochemical interaction between the polymer layer and the surface of iron oxide.^{1,7,8} The mechanism that has been proposed to explain

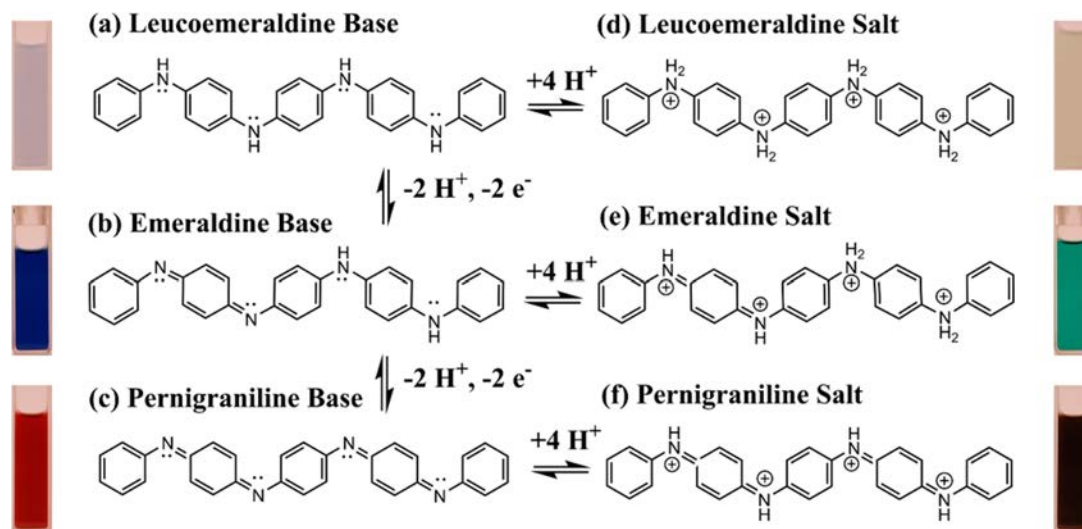
the corrosion inhibition of steel by redox-active organic molecules is based on the assumption that by applying these organic molecules in their oxidized states to metal surfaces they can act as an oxidizers, improving the oxide layer structure by creating a passive oxide.^{1,8} The metal oxide layer remains passivated as long as the organic layer can provide a large enough shift of the corrosion potential. This mainly relies on two conditions: the presence of a sufficient number of active redox-active compounds and the regeneration of reduced organic molecules back into their active form through reoxidation by ambient oxygen.¹

It was recently suggested that limiting the extent of the percolation network present in the organic layer is the key to successful corrosion inhibition, even in the presence of large defects in the organic layer. Rohwerder¹ concluded that an effective redox-active layer should form a microscopic percolation network at the interface rather than a macroscopic one. This means that although good electric contact between the organic film and the passive metal surface is essential,⁹ it is the redox activity of the organic film that is vital for corrosion

Received: October 3, 2016

Revised: December 11, 2016

Published: December 12, 2016

Scheme 1. Chemical Structure and Protonic Doping Process for PCAT^a

^aDoping the base states of oligomers (left) with HCl gas results in the salt state (right). The color of the methanolic solution of each state is visible in the photograph beside each chemical structure.

inhibition and not its electrical conductivity. Instead a macroscopic network of the redox-active polymers leads to fast cation incorporation into the polymer, which results in its fast reduction and thus breakdown of the coating.^{1,10} In addition, the organic layer needs to provide enough passivation current to polarize the surface in order to create a passive oxide layer. Otherwise, the corrosion process would be accelerated more than in the absence of an organic coating.¹ This condition can be achieved through the careful choice of organic molecules. Oligoanilines have emerged as promising substitutes for PANI in corrosion inhibition applications.¹¹ They show the same redox properties, higher solubility, and better processability than PANI. In addition, there is plenty of room for tailoring their structure to achieve the desired properties.¹² It has also been reported that oligoanilines can show superior corrosion inhibition to PANI.¹³ The phenyl-capped aniline tetramer (PCAT, Scheme 1) is the smallest oligomer with at least three oxidation states: leucoemeraldine base (LB, fully reduced state), emeraldine base (EB, half-oxidized state), and pernigraniline base (PB, fully oxidized state).¹⁴

Temperature-programmed desorption mass spectrometry, UV-vis absorption spectroscopy, and X-ray photoelectron spectroscopy (XPS) have already shown the possibility of the vacuum deposition of PCAT on a quartz substrate under high vacuum conditions.¹⁵ In addition to the superior processability, PCAT is reported to lack order in its monolayers because of the number of isomers available for each of its oxidation states.¹⁶ This disordered structure could fulfill the prerequisite for an organic coating with a microscopic percolation network, in the absence of a macroscopic one.¹

Iron naturally forms several different oxide and (oxy)-hydroxide phases when exposed to ambient air and humidity. The oxide layer is not passive and consists of an inner layer of Fe₃O₄ (magnetite) and an outer layer of Fe₂O₃ (hematite or maghemite).^{17,18} The structure of this top layer is of great importance when trying to fully understand the corrosion inhibition of steel by redox-active organic molecules. On occasion, it has been wrongly assumed that the organic coating is in direct contact with the metal phase rather than the native oxide film.^{19,20} However, a thin oxide film consisting of a

mixture of magnetite and maghemite was shown to form on an iron surface at room temperature upon exposure to oxygen at pressures of as low as 10⁻⁴ Torr for only 120 s.²¹

Here we report the impact of the interaction of iron oxide on the redox chemistry and electronic properties of different oxidation states of PCAT. The hematite single-crystal (1000) surface was considered to be a model system. The charge transfer and extent of doping were quantified using X-ray photoelectron spectroscopy (XPS). Changes in the oxidation states of oligoaniline were characterized using Raman spectroscopy. We also investigated the impact of protonic doping on the doping level of base oligoanilines films at an interface with iron oxide. Finally, we examined these interaction/charge-transfer processes between iron oxide and different oxidation states of PCAT through *I*-*V* measurements made by employing an array of interdigitated gold electrodes covered with a thin layer of iron oxide placed inside a microfluidic channel carrying a flow of PCAT solution. The details of these interfacial interactions are crucial pieces in the puzzle of corrosion inhibition and allow for the design of redox-active electronic devices such as chemical sensors.

EXPERIMENTAL DETAILS

PCAT in the leucoemeraldine oxidation state (PCAT LB) was synthesized according to a literature procedure.¹⁴ PCAT in its half-oxidized (PCAT EB) and fully oxidized (PCAT PB) states were prepared using ammonium persulfate (NH₄)₂S₂O₈ (Sigma-Aldrich) as an oxidizing agent. For the preparation of PCAT PB, an excess amount of ammonium persulfate was used. Although the preparation of an exactly half-oxidized state of the oligomers is not possible through chemical doping,⁸ a 1:1 molar ratio of (NH₄)₂S₂O₈ to PCAT LB was used to approximately prepare this oxidation state. To remove the excess amount of oxidizing agent, both solutions were filtered and washed several times with Millipore water (18.2 MΩ cm) under vacuum suction. To ensure that PCAT LB is also in the fully reduced state, the as-synthesized PCAT LB powder was mixed with an excess amount of L-ascorbic acid (Caledon Laboratories Ltd.). The same purification and filtration process applied to PCAT EB and PCAT PB powders was applied to

this sample. Finally, all samples were suspended in a dilute solution of NH_4OH (0.1 mol/L) in order to ensure that they are in the base state. All particles were collected by vacuum filtration using an air aspirator.

Hematite single crystals (natural source, one-side epi polished, SurfaceNet GmbH) with a surface orientation of (1000) were washed with methanol (MeOH, HPLC, Caledon Laboratories Ltd.) and Millipore water. All crystals were exposed to UV–air plasma under low vacuum for 2 min. None of the iron oxide substrates were sputter cleaned prior to deposition of the organic film, as this can cause the reduction of iron oxide.²² Iron(III) oxide nanoparticles (Sigma-Aldrich) with an average particle size of 50 nm were used for Raman measurements. Nanoparticles were annealed in an air atmosphere at 440 °C for 14 h in order to form a hematite phase and remove any organic residue (Figure S5). All organic thin film depositions were performed in a home-built vacuum deposition chamber equipped with a low temperature K-cell, stage cryostat, and deposition monitor (QCM). To minimize cross contamination, the vacuum chamber was thoroughly baked prior to each deposition process. The base pressure of the chamber was better than 5×10^{-6} Torr during all depositions. All samples were stored in a dry nitrogen atmosphere prior to transfer to the UHV analysis chamber. NaCl (reagent grade, Caledon Laboratories Ltd.) was exposed to sulfuric acid (reagent grade, 98.5%, Caledon Laboratories Ltd.) in order to create water-free high-purity HCl vapor used for the protonic doping of PCAT base films on the hematite substrates.

XPS probes the surface of the sample to a depth of 7–10 nm and has detection limits ranging from 0.1 to 0.5 atom %, depending on the element. A Kratos Axis Ultra spectrometer with a monochromatic Al K α X-ray source (15 mA, 1486.6 eV) was used to record the photoelectron spectra of the powders and coated organic films fabricated on glass or a hematite substrate. The PCAT base powders were pressed onto double-sided adhesive tape for XPS analysis. The bare hematite samples were charge corrected to a binding energy (B.E.) of 284.8 eV for C–C and C–H. All of the other samples had the main line of the carbon being mostly C=C, and as such they were charge corrected to the B.E. of 284.5 eV. High-resolution (0.1 eV) spectra were obtained using a 20 eV pass energy and an analysis area of $300 \times 700 \mu\text{m}^2$. All acquired spectra were analyzed using CasaXPS software (version 2.3.17).²³ For peak integration, a Shirley-type background and a line shape of GL(30), which is 30% Lorentzian and 70% Gaussian, were used. Standard deviations of XPS peak areas were calculated using a built-in procedure in Casa XPS software to estimate the precision error of output quantities by optimizing a set of peak parameters.²³

A Renishaw inVia laser Raman spectrometer was used to acquire spectra over a range of 100–1800 cm^{-1} , with a spectral resolution of 2 cm^{-1} , using a 20 \times objective excited with an Ar⁺ ion laser at 514 nm (2.41 eV) or a solid-state laser at 785 nm (1.57 eV). All samples were cast and dried on glass substrates. Data was collected on multiple locations on each sample and recorded with fully focused 1 or 5% laser power having a field of view of $50 \times 50 \mu\text{m}^2$. This will introduce less than 0.4 $\mu\text{W}/\mu\text{m}^2$ for the 514 nm laser beam and 6 $\mu\text{W}/\mu\text{m}^2$ for the 785 nm laser beam into the sample, which minimizes sample damage.²⁴ All Raman spectra were normalized on the basis of their most intense peaks.

Atomic force microscopy was performed in a dry nitrogen atmosphere in tapping mode using a Veeco Enviroscope with a Nanoscope IIIa controller. Typical line scan rates were 0.5 Hz. Care was taken to ensure that the tip was not modifying the surface during image acquisition. For all images, the background was subtracted and the lines were corrected by matching median height levels using Gwyddion data analysis software.²⁵

The microfluidic devices are fabricated by first sputter depositing a 200 nm gold film on a glass slide. Then an array of 500 interdigitated electrodes with 100 μm spacing was photolithographically patterned. Next, a 14.2 nm iron oxide film was deposited on the gold electrodes under high-vacuum conditions (base pressure $\sim 5 \times 10^{-6}$). The iron source was a clean iron wire (0.99%, diameter = 0.01 cm, OMEGA Engineering) wrapped tightly around a clean tantalum wire. To form iron oxide, pure oxygen gas (oxygen 2.6 grade, BOC Canada Limited) was introduced into the vacuum chamber through a leak valve ($P = 5 \times 10^{-4}$ Torr) during the slow evaporation of the Fe source (~ 1 nm/min), as monitored by QCM. Subsequently, the substrate was exposed to hydrogen peroxide vapor for over an hour to ensure that the deposited film was oxidized. A poly(dimethylsiloxane) (PDMS) microchannel (length/width/depth = 50 mm:5 mm:100 μm) was fabricated by soft lithography. Subsequently, the PDMS microchannel was bonded on top of interdigitated electrodes by air plasma. Conductivity measurements were carried out using a Keithley 2636 source measuring unit.

RESULTS

Film Fabrication Method. Prior to studying the interaction of oligoanilines with iron oxide surfaces, it is crucial to know the possible effects of the organic layer's fabrication methods on its chemical state. Two common fabrication methods for small-molecule thin films are drop casting^{12,26} and vacuum deposition.¹⁵ Vacuum deposition has the benefit of controlling the film thickness with subnanometer precision, but the process involves expensive instrumentation.^{15,27} On the other hand, drop casting is simple, and the morphology and crystallinity of the film can be altered on the basis of the choice of the solvent, nonsolvent, and substrate; however, there is poor control over the thickness of the film.²⁶

High-resolution XPS was utilized to examine the impact of the deposition method on the chemical state of the organic films as well as pristine powders. The LB (Scheme 1a) and PB (Scheme 1c) states of PCAT contain only benzenoid nitrogen (amine structure) and quinonoid nitrogen (imine structure), respectively, whereas the EB state of PCAT (Scheme 1b) consist of equal amounts of these structures. Thus, the oxidation states of PCAT can be assessed on the basis of the percentage of amine and imine groups. Therefore, the N 1s XPS spectra of the pristine PCAT LB, PCAT EB, and PCAT PB powders were obtained to use as reference spectra for this work.

The N 1s spectrum of the pristine PCAT LB powder (Figure 1a) exhibits only a symmetrical peak at 399.5 eV. This peak is characteristic of neutral amine nitrogen ($-\text{NH}-$ structure)^{28,29} and shows that the powder is in the fully reduced state as expected. The XPS N 1s envelope peak of PCAT EB powder (Figure 1b) at ~ 399 eV is asymmetric with a distinct shoulder at lower B.E. Deconvolution of this peak yields an amine nitrogen peak at 399.6 eV and an imine nitrogen peak at 398.5 eV. On the basis of the area under these two peaks (65.9%

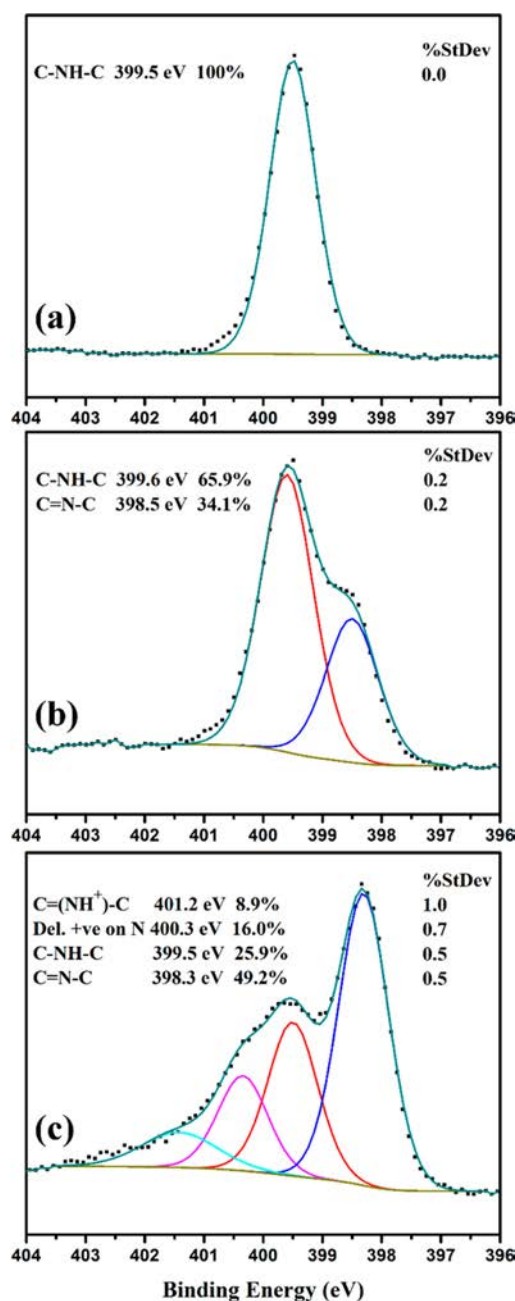


Figure 1. High-resolution N 1s XPS spectra of (a) pristine PCAT LB powder, (b) PCAT EB powder, and (c) PCAT PB powder.

amine nitrogen, 34.1% imine nitrogen), this powder is not exactly half oxidized. Although the EB state should be theoretically 50% oxidized, this result is consistent with previous literature reports for PANI EB⁸ because chemical modification of the organic molecules to an exact intermediate oxidation state is difficult to control.³⁰ The N 1s peak of PCAT PB powder was fitted by four peaks at 398.3, 399.5, 400.3, and 401.4 eV (Figure 1c). The peaks at 398.3 and 399.5 eV are in agreement with the B.E.²⁹ of the nitrogen atoms in imine and amine structures, respectively. On the basis of the previous reports, the other two peaks at higher B.E.s can be assigned to charged nitrogen species.^{3,32} The peak at 400.3 eV was attributed to the nitrogen atom with delocalized positive charge,³¹ and the one at higher B.E. (401.4 eV) was assigned to the N⁺ atom in C=(NH⁺)–C.^{31–33} On the basis of the area

under the amine peak, the powder was less than three-quarters oxidized. The presence of two peaks associated with positively charged nitrogen atoms is presumably due to the incomplete washing of sulfate or persulfate from the product after the oxidizing step. This argument is supported by the presence of S 2s and S 2p signals in the survey spectra of the PCAT PB powder (Figure S7b) as an indication of a residual amount of sulfate still present in this sample. No such signals have been detected for the PCAT LB powder (Figure S7a).

To minimize the effect of the substrate on the chemical state of the deposited film, glass slides were used as neutral substrates. For the preparation of drop cast films, pristine PCAT LB powder was sonicated in MeOH (~7.9 mM) for 2 min and was cast on glass slides at room temperature. Figure 2a,b shows the N 1s core-level XPS spectra of vacuum-

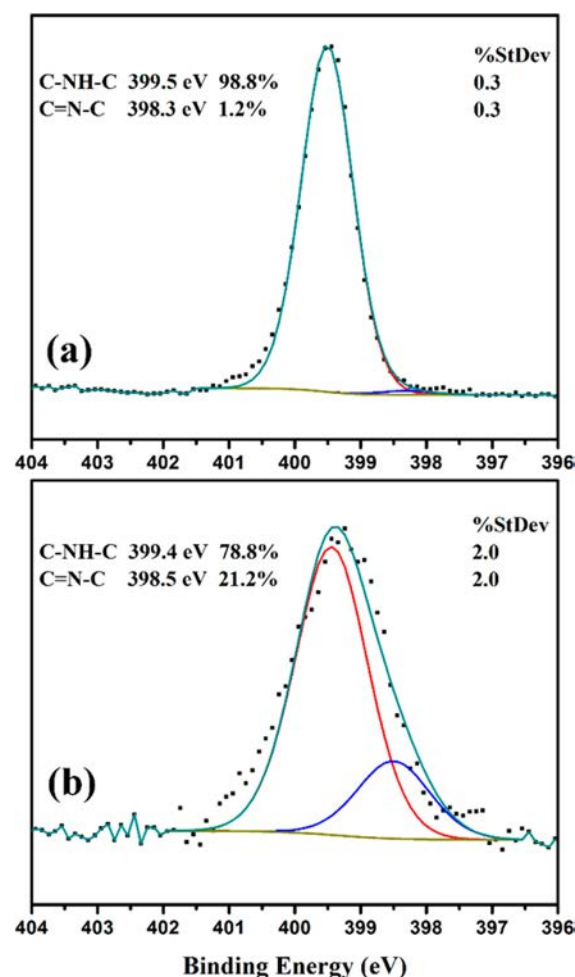


Figure 2. High-resolution N 1s XPS spectra of (a) the PCAT LB film vacuum deposited on a glass substrate and (b) the PCAT LB film drop cast on a glass substrate.

deposited and drop-cast films on glass substrates. The N 1s spectrum of the PCAT LB thin film fabricated by vacuum deposition on glass was deconvoluted into two peaks (Figure 2a). The major peak is an amine peak (399.5 eV). The other fitted peak is a low-intensity imine peak (398.3 eV). This peak makes only about a 1% contribution to the envelope peak. It is also possible to fit the N 1s spectrum of the organic film drop cast on glass (Figure 2b) by an amine (399.4 eV) and an imine peak (398.5 eV). In contrast to the vacuum-deposited film, the

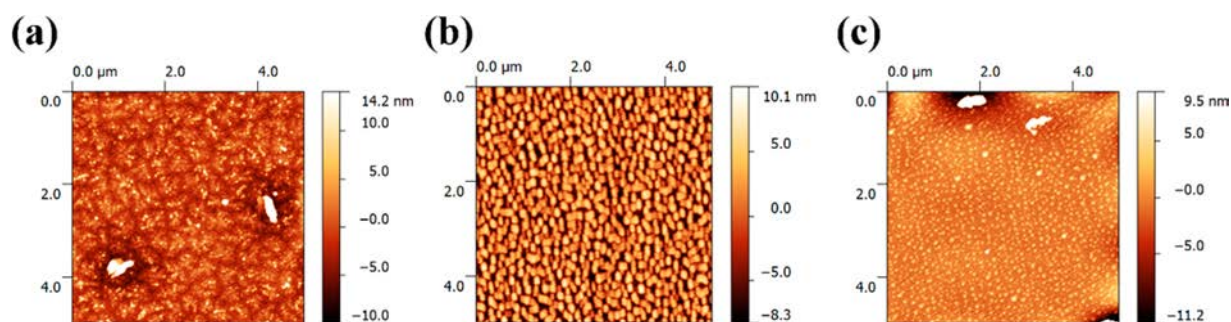


Figure 3. (a) The PCAT LB film (2.5 nm thick) on hematite single crystal ($5 \mu\text{m} \times 5 \mu\text{m}$), (b) the PCAT EB film (2.5 nm thick) on hematite single crystal ($5 \mu\text{m} \times 5 \mu\text{m}$), and (c) the PCAT PB film (2.3 nm thick) on a hematite single crystal ($5 \mu\text{m} \times 5 \mu\text{m}$).

contribution of the imine peak to the envelope peak was increased to more than 20%. This partial oxidation may be due to the prolonged exposure of the PCAT film to ambience during the sonication, deposition, and drying process. A comparison of the deconvoluted N 1s XPS spectra shows that vacuum deposition has a negligible effect on the oxidation states of the pristine PCAT powder whereas drop casting can cause a considerable change in the oxidation state of the precursor. Therefore, on the basis of this experiment and because the thickness of the deposited film can be more precisely controlled through vacuum deposition, this technique was used as the method of choice for the rest of this study, unless stated otherwise.

Morphology of the Oligoaniline Films. There have been several reports on XPS of redox-active organic compounds deposited on steel and iron oxide substrates, attempting to understand the interaction at this interface.^{8,34,35} However, to the best of our knowledge all of these studies used organic films with thicknesses in the range of hundreds of nanometers to micrometers. Because XPS is capable of probing only a few nanometers from the surface, all of these studies are in fact probing the interaction at the interface of the organic compounds and the ambient surroundings or the interactions in the bulk of the organic film. Thus, to ensure that the XPS data includes the signal from the interface of iron oxide and the organic layer, the thickness of the organic layer must be limited to a few nanometers. The deposition conditions (substrate temperature and deposition rate) were optimized in order to fabricate thin and uniform organic films. The thickness and morphology of each layer were studied by AFM. Vacuum-deposited PCAT, in its fully reduced state, on a hematite (1000) surface tends to wet the surface and form dendritic islands that are less than 7 nm thick (Figure 3a). The same quality films can be achieved for the PCAT EB film (Figure 3b), although in this case the islands are more globular in shape. Deposition of PCAT PB on the substrate kept at room temperature ($\sim 25 \text{ }^\circ\text{C}$) led to the formation of two types of island morphology; small, thin, globular islands and long, thick, needle-shape islands (Figure S8). By keeping the substrate at lower temperatures during the deposition ($9\text{--}10 \text{ }^\circ\text{C}$), the number of needle-shaped islands decreases (Figure 3c). Thus, the latter condition is preferable, as it leads to the formation of a more uniformly thin organic layer. This variation in the morphology of the islands is an indication that PCAT PB molecules tend to dewet the surface more than PCAT LB and EB molecules do, likely because of weaker interactions with the surface.

The higher dewetting of the metal oxide surface by PCAT molecules in higher oxidation states differs from the trend

predicted for the aggregation of PANI in organic solutions.³⁶ Zhang et al. reported that the highest extent of self-association is observed for the EB state because of the possibility of interchain hydrogen bonding between imine and amine nitrogen sites. Because of the fact that the LB and PB states consist only of purely amine or purely imine groups, respectively, no such aggregation should be expected. Island formation of oligoanilines on solid metal oxide surfaces depends on the balance of molecule–surface and molecule–molecule interactions. Water adsorption and dissociation on iron oxide surfaces, including hematite, leads to the formation of hydroxyl groups at different surface sites,^{37–39} aiding the interaction with the PCAT molecules through their amine and imine groups. For PCAT LB, the lone pair electrons of amine nitrogen can interact with the hydrogen of the surface hydroxyl groups, in addition to the interaction between the lone pair of electrons of the oxygen in the hydroxyl groups and the hydrogen in the amine group. In the case of PCAT PB, the lone pair of the imine nitrogen can interact with the hydrogen in the hydroxyl group. This decrease in the interaction pathways between the oxidized molecules and the substrate can account for the lesser degree of surface wetting by PCAT PB and PCAT EB films.

Interaction of PCAT LB with the Hematite Surface.

Thin films of PCAT LB were vacuum-deposited on hematite single-crystal substrates. A bare hematite substrate was used as a reference sample for the Fe 2p spectra. For all samples, high-resolution Fe 2p, O 1s, C 1s, and N 1s XPS peaks were collected. Deconvolution of the N 1s envelope peak of PCAT LB-coated hematite shows three peaks (Figure 4): a primary amine peak at 399.5 eV and two minor peaks at 398.3 and 401.2 eV. The component at 398.3 eV can be assigned to imine ($=\text{N}-$ structure).²⁹ As previously reported for PANI,^{32,33} the higher B.E. component of the N 1s envelope peak was attributed to the most positively charged nitrogen sites ($\text{C}=(\text{NH}^+)-\text{C}$ structure). On the basis of this peak assignment, the N 1s envelope peak consists of approximately 93% amine nitrogen, 5% positively charged nitrogen, and 2% imine. A comparison of these spectra with the N 1s XPS spectra of PCAT LB powder as a reference sample (Figure 1a) indicates the partial oxidation of PCAT LB on hematite. In addition, even though there are reports on the X-ray-induced reduction of materials in UHV,^{40,41} no such reduction was observed in the case of PCAT LB on hematite by comparison to the N 1s XPS spectra of PCAT LB powder.

Raman spectroscopy is an alternative tool to characterize the interaction between these oligoanilines and iron oxide surfaces. Under ambient conditions, it is a powerful tool to qualitatively determine the oxidation states of PANI and its oligomers.⁴²

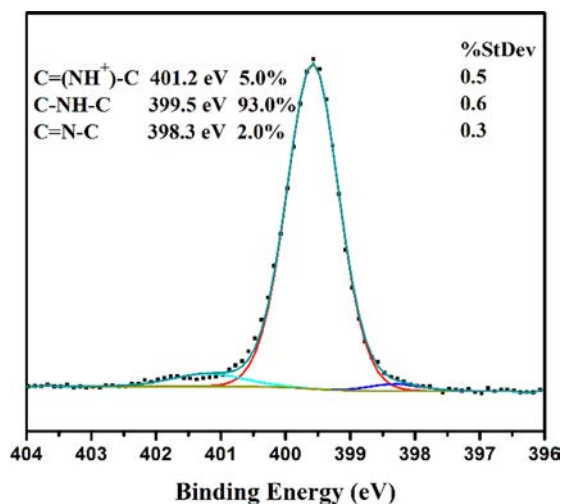


Figure 4. High-resolution N 1s XPS spectra of PCAT LB deposited on a hematite surface.

Because normal Raman spectroscopy lacks the surface sensitivity of XPS, acquiring a strong Raman signal from the few monolayers in direct contact with the hematite surface is nontrivial. One way to amplify this signal is by increasing the surface area of the interface between the organic layer and the metal oxide. Therefore, instead of using a flat single-crystal surface, small iron oxide nanoparticles with a mean diameter of 50 nm were used. PCAT LB powder was mixed with the annealed hematite nanoparticles (1:5 by weight) using a vortex mixer. Both pristine PCAT LB powder and the mixture were sonicated in MeOH for 10 min and were cast onto glass slides. Because Raman features are known to be sensitive to many parameters including temperature and laser power,^{24,43} the lowest possible laser power (below $0.4 \mu\text{W}/\mu\text{m}^2$) was utilized during spectra acquisition. For comparison, the most intense peak of each spectrum was normalized to 1. The PCAT LB film showed the three main signature Raman bands of the reduced state of PCAT at 1179, 1221, and 1622 cm^{-1} (Figure 5a).^{44,45} No bands indicating the presence of the other oxidation states of PCAT are observed. For the mixture of hematite nanoparticles with PCAT LB, all three bands observed for

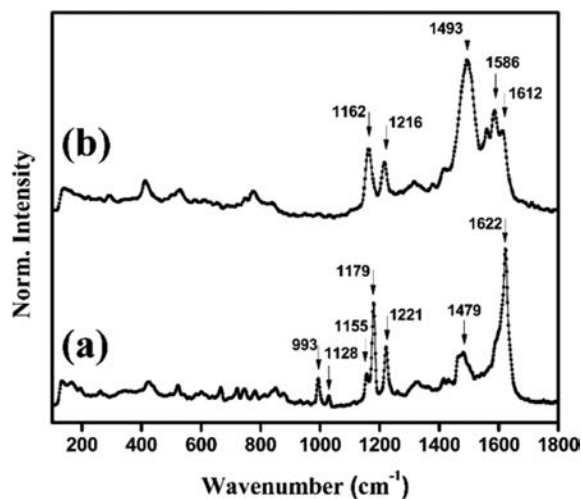


Figure 5. Raman spectra of (a) the PCAT LB film and (b) the composite film of PCAT LB and hematite nanoparticles.

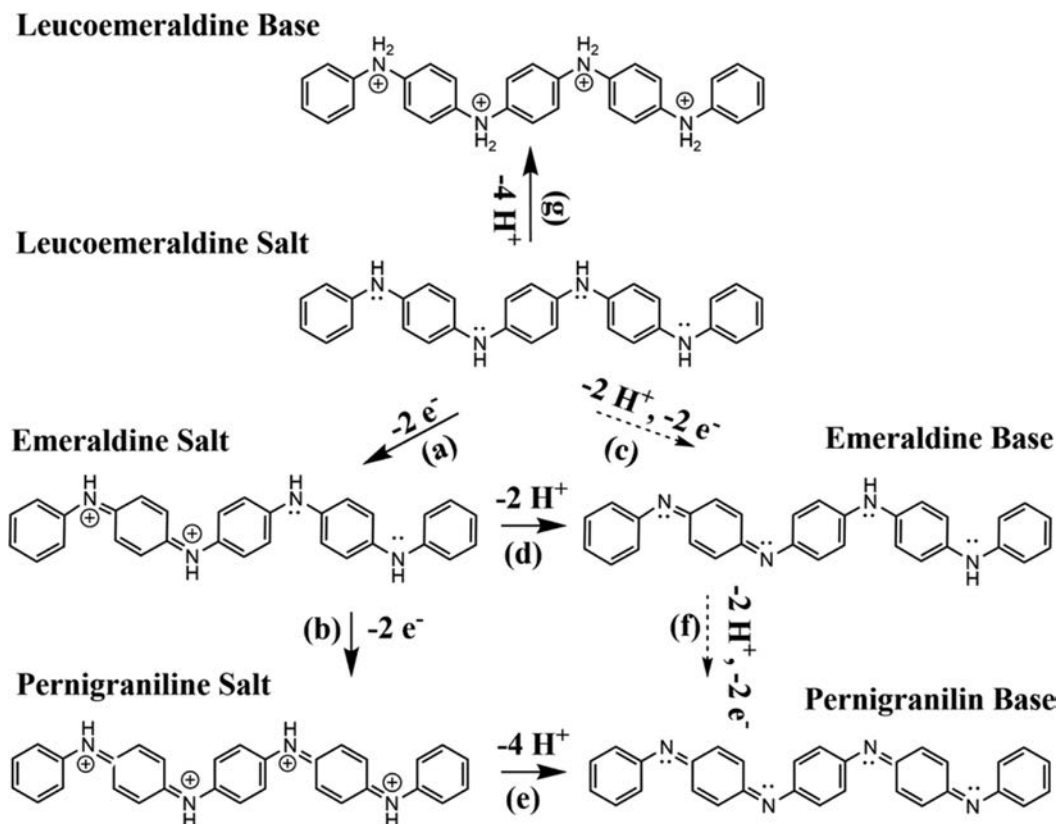
the pristine PCAT LB disappeared and instead five bands at 1162, 1216, 1493, 1586, and 1612 cm^{-1} emerged (Figure 5b). These bands are associated with the oxidation of PCAT.⁴⁴ The coexistence of these bands and the low-intensity bands of PCAT LB proves the partial oxidation of PCAT LB at the surface of hematite particles.

Both Raman spectroscopy under ambient conditions and XPS in vacuum indicate the partial oxidation of PCAT on hematite. Scheme 2 depicts different pathways for oxidation/reduction and doping/dedoping of PCAT. On the basis of this scheme, one route for the oxidation of PCAT LB is losing two electrons and two protons, and thus the product of this process remains in the base state (Scheme 2c). The other possibility is the oxidation of the oligoanilines mediated by the hematite surface. The removal of electrons from a base form of amine nitrogen through charge transfer to hematite and the formation of a positivity charged amine nitrogen is also an oxidation process. The result of such a process is the salt form of the molecule (Scheme 2a). Hence, the hematite surface can oxidize PCAT LB as an alternative process to the oxidation of the leucoemeraldine state under ambient conditions.⁸ It has been known that polyaniline can be oxidized on the surface of iron oxide by oxygen.⁴⁶ Although extreme care has been taken to minimize the exposure of the sample to air, this could be an alternative source of oxidation of PCAT LB, as the sample has been exposed to the laboratory atmosphere for a short amount of time during the transfer from the deposition chamber to the XPS chamber.

In Situ Deposition and Spectroscopy of PCAT LB on Low-Carbon Steel. To examine whether the oxidation of the PCAT LB film on hematite was induced by the interfacial interactions, the previously reported high-resolution XPS spectra of the in-situ-deposited LB on a sputtered clean steel substrate were reanalyzed.¹⁵ The layer-by-layer deposition of LB had been performed in three different thicknesses with the final thickness of approximately 5 nm. The N 1s XPS spectrum of the sputtered cleaned steel shows a low-intensity spectrum of nitrogen species at around 396.8 and 400.5 eV (Figure 6a). The former peak is attributable to nitride compounds formed as a result of the sputtering process of the steel. The latter peak is indicative of an unknown organic nitrogen, possibly amide.¹⁵ After the first deposition of LB (Figure 6b), two additional peaks appear, an amine peak at 399.4 eV (53.89%) and an imine peak at 398.2 eV (17.75%). After further deposition of LB, the N 1s spectrum still can be deconvoluted into the same three peaks (Figure 6c). The contribution of the amine peak to the envelope peak increases (64.48%), and the contribution of the imine peak decreases (13.98%). Finally, after the deposition of approximately 5 nm of LB on steel, the N 1s envelope peak can be deconvoluted only to a major amine peak (99.13%) and a minor imine peak (0.87%) (Figure 6d).

Because the deposition and XPS analysis had been performed in two interconnected vacuum chambers, the sample had not been exposed to ambient conditions prior to data acquisition. These results indicate that the partial oxidation of the thin LB film on steel is mediated by iron oxide. It also confirms that the LB film was indeed partially oxidized through interaction with iron oxide (Figure 4). In addition, using ultraviolet photoelectron spectroscopy, it has been shown that the deposition of a thin film of fully reduced PCAT on steel causes band bending and a decrease in the work function of the metal oxide surface by 0.5 eV.¹⁵ This makes it easier for LB to be oxidized on the surface of iron oxide. This observation is consistent with our

Scheme 2. Conversion between Different Base and Salt States of PCAT at the Interface with Hematite



results regarding the oxidation of PCAT LB on hematite as obtained by XPS and Raman spectroscopy. As the thickness of the LB film reaches approximately 5 nm, the contribution of the imine to the N 1s peak decreases. The imine species remain localized at the interface. Further deposition of PCAT results in the attenuation of the signal from the interface. The nitrogen in the newly deposited layer retains its amine character.

This shows that the interface-mediated charge transfer by the iron oxide is limited to the proximity of the interface in comparison to air oxidation, which can act on the bulk organic film. The comparison of the N 1s spectra of the LB film on steel with the same film on a hematite single crystal shows the absence of charged nitrogen peaks at higher B.E. in the former sample. One possible reason behind this discrepancy could be the differences in the chemical and electronic properties of the low-carbon steel and hematite single crystal. The other major difference between these two samples is the adsorbed water film on their surfaces. The hematite single crystal had been exposed to the ambient environment, which allows for the formation of a water film on the substrate. The presence of such a film on this particular steel substrate is less likely due to oxidation under dry nitrogen flow.

Interaction of PCAT EB and PCAT PB with the Hematite Surface. The same characterization methodology applied to the PCAT LB-hematite interface was repeated for other oxidation states of PCAT. Thin films of PCAT EB and PCAT PB fabricated on hematite single-crystal substrates were studied by XPS. The N 1s XPS spectrum obtained from the interface of a PCAT EB film and hematite can be fitted by three peaks (Figure 7a). The peaks at 399.56 and 398.3 eV were assigned to amine and imine nitrogen, respectively, and the peak at 401.2 eV was assigned to positively charged nitrogen as

previously reported for PANI in contact with graphene.^{32,33} As for the interface between PCAT LB and hematite, this peak is a sign of charge transfer between the PCAT EB film and hematite. A comparison of the area under these fitted peaks with the deconvoluted spectra of the PCAT EB powder (Figure 1b) shows that the interaction of the PCAT EB molecules with hematite leads to the partial reduction of PCAT.

Deconvolution of the N 1s peak for the PCAT PB-coated hematite (Figure 7b) leads to the same four peaks that were previously fitted for the N 1s XPS spectrum of PCAT PB powder (Figure 1c). However, the contribution of each peak to the envelope peak has changed significantly. Figure 8b shows that the intensity of the amine peak increased drastically at the expense of the imine peak in the PCAT PB powder (Figure 1c). This demonstrates a significant reduction of the fully oxidized oligomers in contact with the hematite phase. However, the number of charged nitrogen atoms was slightly decreased. Therefore, the deconvoluted N 1s XPS spectra of PCAT EB and PCAT PB films on hematite substrates show the partial reduction of the small molecules in addition to the interfacial charge transfer at the interface.

Raman spectroscopy of PCAT EB and PB powders mixed with hematite nanoparticles confirmed the results obtained from XPS. Raman spectra of pristine PCAT EB (Figure 8a) and a mixture of PCAT EB and hematite nanoparticles (Figure 8b) look almost identical, and both show Raman bands at approximately 1162, 1214, 1496, and 1585 cm^{-1} . These bands are associated with PCAT in its half-oxidized state.⁴⁴

The Raman spectra of PCAT PB powder (Figure 8c) and the composite film of PCAT PB and hematite nanoparticles (Figure 8d) show several bands of oxidized PCAT. However, the transformation of the shoulder of the bands at 1589 and

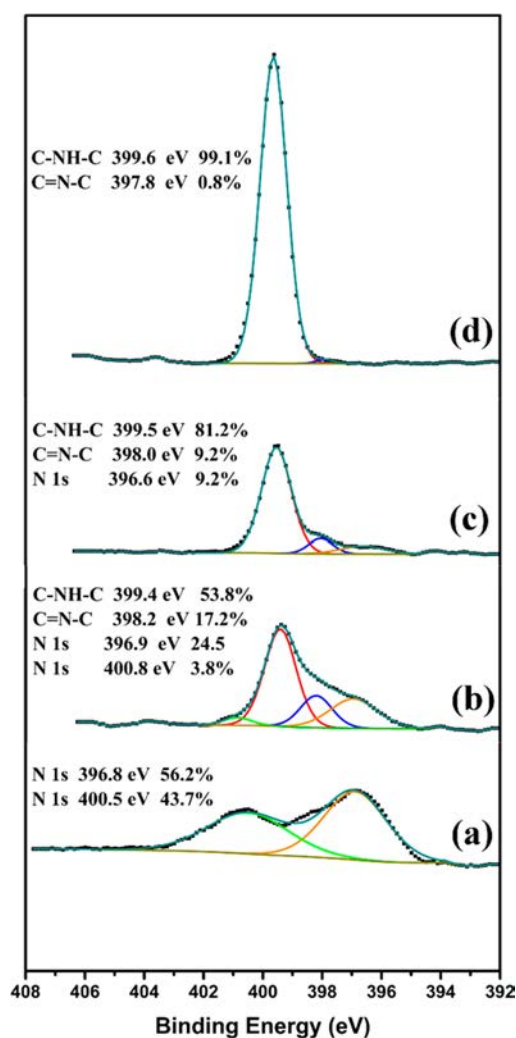


Figure 6. High-resolution N 1s XPS spectra of (a) sputtered, cleaned low-carbon steel, (b) PCAT LB first deposition, (c) PCAT LB second deposition, and (d) PCAT LB third deposition on steel.

1500 cm^{-1} in the PCAT PB powder spectrum to the separate bands at 1619 and 1488 cm^{-1} in the mixture of PCAT PB with hematite, respectively, can be interpreted as the sign of the partial reduction of PCAT.⁴⁴ One reason behind the greater similarity between the Raman spectra of the PCAT PB and its mixture with hematite nanoparticles is the fact that the measurement has been performed in air and thus there is a possibility of air-exposed oxidation. In addition, the observation of this reduction event by both XPS and Raman spectroscopy is an indication that this reduction was not induced by the X-ray beam used in XPS.

The XPS spectra presented here (Figure 7a,7b) indicate that the thin films of PCAT EB and PB will be reduced by hematite surfaces. The presence of N 1s signals at higher B.E. indicates the possibility of charge transfer at the interface between oxidized molecules (PCAT EB or PB) and the hematite substrate. Raman spectroscopy, under ambient conditions, also shows a partial reduction of PCAT PB molecules in contact with hematite nanoparticles. No such reduction was observed for PCAT EB molecules. These results are consistent with the previously assumed mechanism for corrosion protection of steel by redox-active organic compounds.⁸ It has been argued that these compounds, if applied in their oxidized states, can act as

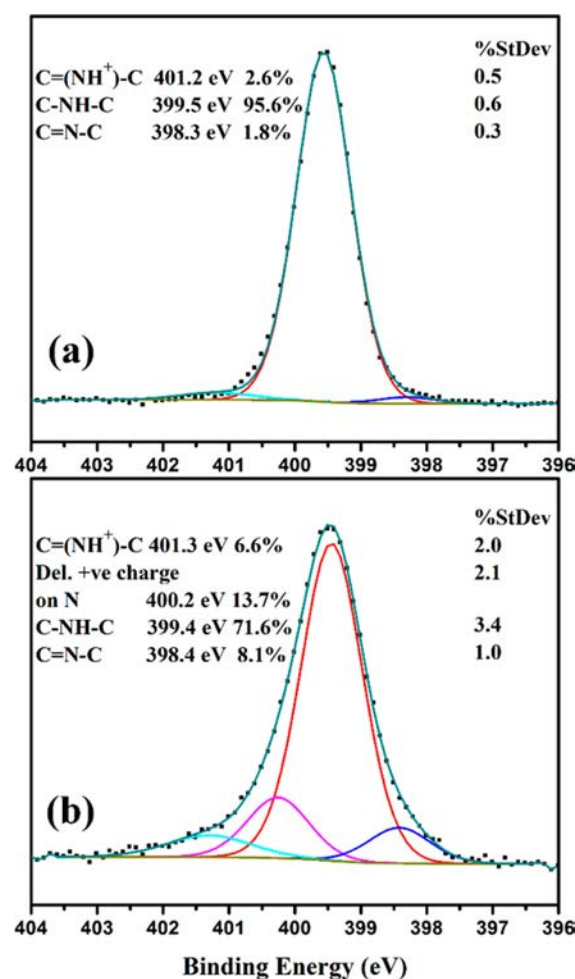


Figure 7. High-resolution N 1s XPS spectra of (a) PCAT EB deposited on a hematite surface and (b) PCAT PB deposited on a hematite surface.

an oxidizer, improving the underneath metal oxide layer and inhibiting the corrosion. However, these reports assumed EB to be the oxidized form whereas it is only half-oxidized.^{8,34} In addition, the organic films used in those cases were several micrometers thick.⁸ The base forms of PANI and its oligoanilines are known to be extremely poor electrical conductors. Therefore, it is expected that most of these measurements benefit not only from corrosion inhibition induced by redox-active organic compounds in proximity to the interface but also from other mechanisms such as barrier coating protection. Our results expand the understanding of corrosion inhibition by redox-active organic compounds by using the fully oxidized PCAT (PB) instead of half-oxidized PCAT (EB). In addition, using only very thin films for the organic coatings ensures that the observed change in the organic phase was indeed induced by the underlying metal oxide surface.

Interaction of PCAT Salt with Hematite Surfaces. Even though there are reports on effective corrosion inhibition using redox-active organic compounds in their base form,^{42,47,48} most of the research to date is focused on the application of the salt form of these compounds.^{49–51} This is based on the assumption that the higher conductivity of the salt films will assist with better integration of the entire organic layer and thus more effectively passivate any exposed metal.^{19,52} Kinlen et

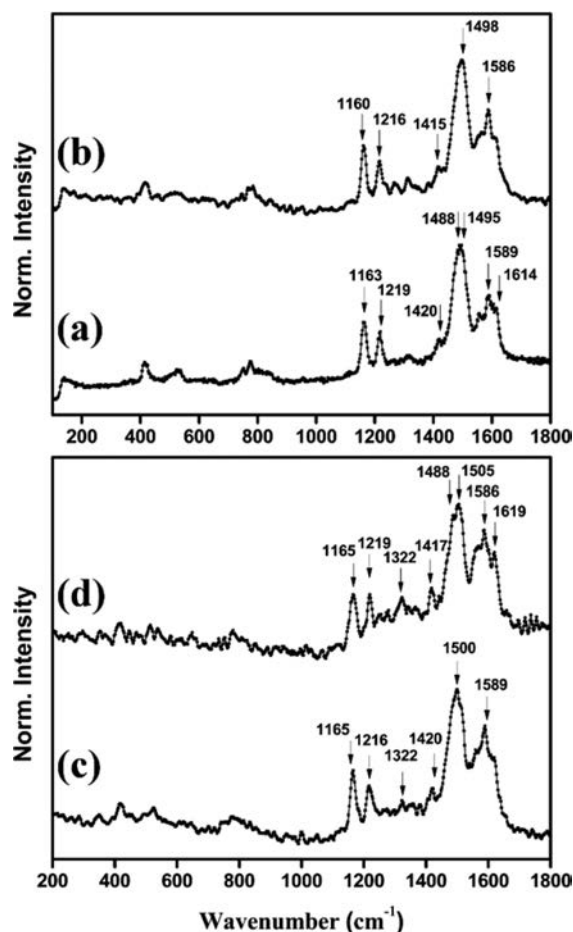


Figure 8. Raman spectra of (a) the PCAT EB film, (b) the composite film of PCAT EB and hematite nanoparticles, (c) the PCAT PB film, (d) the composite film of PCAT PB and hematite nanoparticles.

al.^{42,46} have suggested that the conversion of ES state films fabricated on steel to LS state films is done through redox chemistry and to EB state films through acid–base means. It is not possible to directly deposit the salt form of PCAT in vacuum. Therefore, to fabricate thin and uniform films of PCAT salt, all of the previously analyzed PCAT base films on hematite were exposed to gaseous HCl for 30 s and load-locked back to the XPS chamber. The N 1s XPS spectra of PCAT LS (Figure 9a) still can be properly fit by three peaks of an imine (398.5 eV), an amine (399.5 eV), and a positively charged amine ($-\text{NH}^+$, 401.2 eV). Although the quantitative comparison of these peaks with the N 1s spectra of PCAT LB on hematite shows only a slight increase in imine content, there is a more than a 2-fold increase in the number of charged amines. This expected increase in the amount of cationic nitrogen in PCAT salt is due to protonic doping by HCl gas. The Cl 2p XPS peak from this sample (Figure S17) can be decomposed into a $2p_{3/2}$ peak at 198.4 eV and a $2p_{1/2}$ peak at 200.0 eV. These peaks are attributed to the presence of chloride species in the vicinity of nitrogen atoms in the structure of PCAT. The absence of any peaks at higher B.E.s is a sign that no covalently bonded chlorine was formed upon exposure to HCl gas and thus is proof of the successful protonic doping of PCAT.⁵³

A comparison of N 1s XPS spectra of the PCAT EB film on hematite before (Figure 7a) and after (Figure 9b) exposure to HCl gas shows the appearance of a fourth peak at 400.2 eV. On

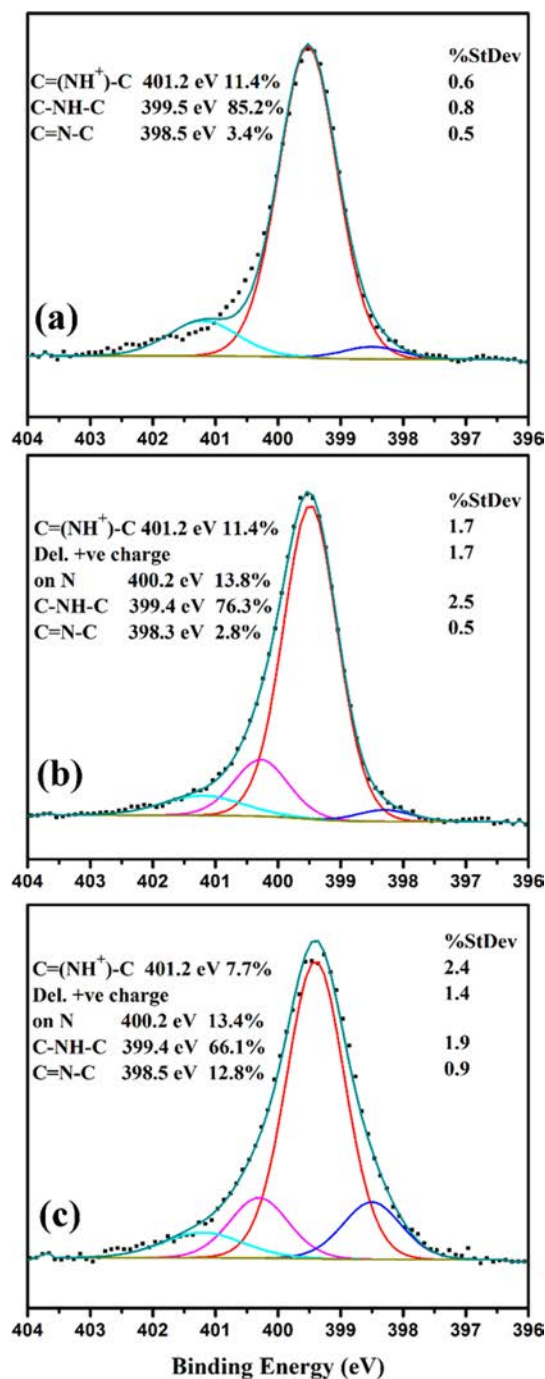


Figure 9. N 1s XPS spectra of salt PCAT on hematite for (a) PCAT LS, (b) PCAT ES, and (c) PCAT PS.

the basis of a previous report on PANI, this peak was assigned to the delocalized positive charge on the backbone of the oligomer.²⁹ This new peak has the second highest contribution to the envelope peak after the peak of the benzenoid nitrogen. Although protonic doping does not lead to a significant increase in the amount of imine nitrogen, the amount of positively charged nitrogen tripled.

The same number of fitted peaks, with the same trend between the doped (Figure 9c) and undoped (Figure 7b) organic films on hematite, has been observed for the fully oxidized form of PCAT. On the basis of the previous reports on the interaction of PANI and graphene,^{32,33} the N 1s XPS signals

at higher B.E.s such as 400.4 and 402.0 eV are associated with the electronic interaction between the two materials and were considered to be a sign of the protonic doping process at the interface.

Because all three PCAT base films (LB, EB, PB) fabricated on the hematite substrate have been exposed to the same amount of HCl gas for the same period of time, the only difference between the salt films is the starting base structure from which they are derived (imine and amine content). The amount of amine and imine structure between the base PCAT LB and EB films on hematite and their corresponding salt films (LS and ES, respectively) stayed nearly constant, whereas the content of charged nitrogen has been significantly increased. Although the comparison of the PB and PS films on hematite shows only a slight increase in the amount of imine after exposure to HCl gas, the amount of charged nitrogen stayed the same in both samples. This comparison between the base and salt films shows that the PCAT films exposed to excess HCl gas do not show more than an $\sim 20\%$ cationic nitrogen N 1s signal. One way to determine the protonic doping level of each film is through the ratio of Cl/N atomic percentages, derived from the area under their peaks. On the basis of this method, PCAT LB and PB are doped to almost the same level (25.0 and 25.9%, respectively), whereas PCAT EB was doped to a lesser degree (18.9%). Another way to determine the extent of protonic doping is by considering the ratio of charged nitrogen atoms to the total amount of nitrogen. On the basis of this method, the PCAT EB and PB films are doped almost twice as much (20.8 and 21.1%, respectively) as the LB film (11.4%). The results from the later method are in better agreement with the expected structures in Scheme 2, which shows the increase in protonic doping by moving toward oxidized states. This is due to the fact that the ratio of Cl/N atomic percentages includes all Cl⁻ ions, some of which might not participate in the protonic doping process.

Impact on the Substrate. In the case of the protonation of the PCAT LB organic layer and its partial oxidation by hematite, a partial reduction of iron oxide and the alteration of its oxidation state should be observed. The B.E. of O 1s is independent of the Fe oxidation states and thus cannot be used to monitor the effect of charge transfer on the hematite substrate (Figure S8).^{54,55} Different iron oxide and hydroxide phases are commonly distinguished by their Fe 2p XPS spectra.⁵⁴ However, the analysis of Fe 2p spectra is challenging because of issues such as peak asymmetry, complex multiplet splitting, and overlapping B.E.s.²² The Fe 2p spectra of both the bare hematite surface (Figure 10a) and the hematite surface coated with PCAT LB (Figure 5b) exhibit two sets of peaks, 2p_{1/2} (~ 724 eV) and 2p_{3/2} (~ 711 eV), as a result of spin-orbit coupling. They also show Fe 2p_{3/2} and Fe 2p_{1/2} shake-up satellite peaks with B.E.s of around 719 and 733 eV, respectively. On the basis of ref 22, the satellite peaks were omitted from the fitting performed for the 2p_{3/2} part of the spectrum using a Shirley background. For each sample, the envelope peak at ~ 711 eV was deconvoluted into five peaks. The positions, fwhm's, and areas of these peaks confirm the presence of a single hematite phase.²² The absence of a peak at around 706 eV confirms that there is no metallic iron present in either of the samples, as expected in the case of a hematite single crystal.

The Fe 2p satellite peaks can in principle be used to identify if any reduction of Fe³⁺ to Fe²⁺ occurring upon adsorption of PCAT LB Fe³⁺ satellite peaks appear at ~ 719 and 733 eV, in

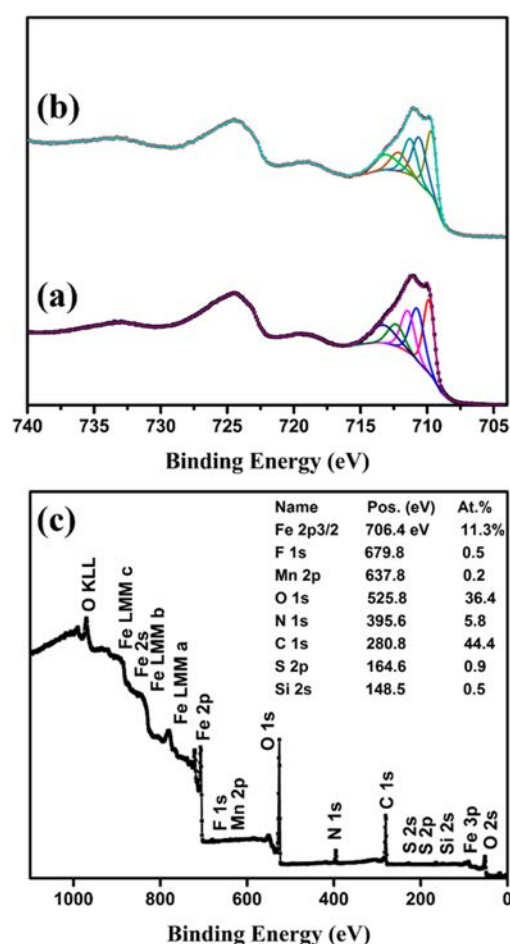


Figure 10. High-resolution Fe 2p XPS spectra of the bare hematite surface (a) before and (b) after vacuum deposition of 2.5-nm-thick PCAT LB film. Both spectra indicate the presence of a hematite phase. (c) XPS survey spectra of the PCAT LB-coated hematite interface.

contrast to Fe²⁺ satellite peaks that are typically found at ~ 716 and 730 eV.^{54,55} Despite a slight shift being observed between the positions of the satellite peaks of the bare hematite and PCAT LB-coated hematite samples, the spectra look largely identical and the shift is possibly due to the uncertainty of using C 1s as a charge-correction reference. The following calculation will demonstrate how this subtle expected change in the hematite phase due to the absorption of an organic layer is below the sensitivity of the XPS instrument used in this work. The Fe 2p and N 1s photoemissions contribute only 11.3 and 5.8% to the XPS survey spectra of the PCAT LB-coated hematite surface (Figure 10c), respectively. From this share of N 1s, only 2.8% of it is associated with the charged nitrogen peak (C=N⁺-C) giving an overall 0.15%. If we assume that all eight nitrogen atoms present in each triclinic unit cell of PCAT are projected onto the interface with the hematite surface in a plane and the α -Fe₂O₃(1000) single crystal has a completely Fe-terminated surface, then there will be an approximately 1:1 interaction between surface Fe atoms and the cationic charged nitrogen.^{56–58} This could lead to about a 1.3% change in the Fe 2p spectra (0.15/11.3: N⁺/Fe 2p). This subtle change is very unlikely to be detectable considering that the data used for such a calculation is not truly coming from an interface but from a few nanometers to each side of it. In addition, the presence of an overlayer (organic layer) results in a background slope

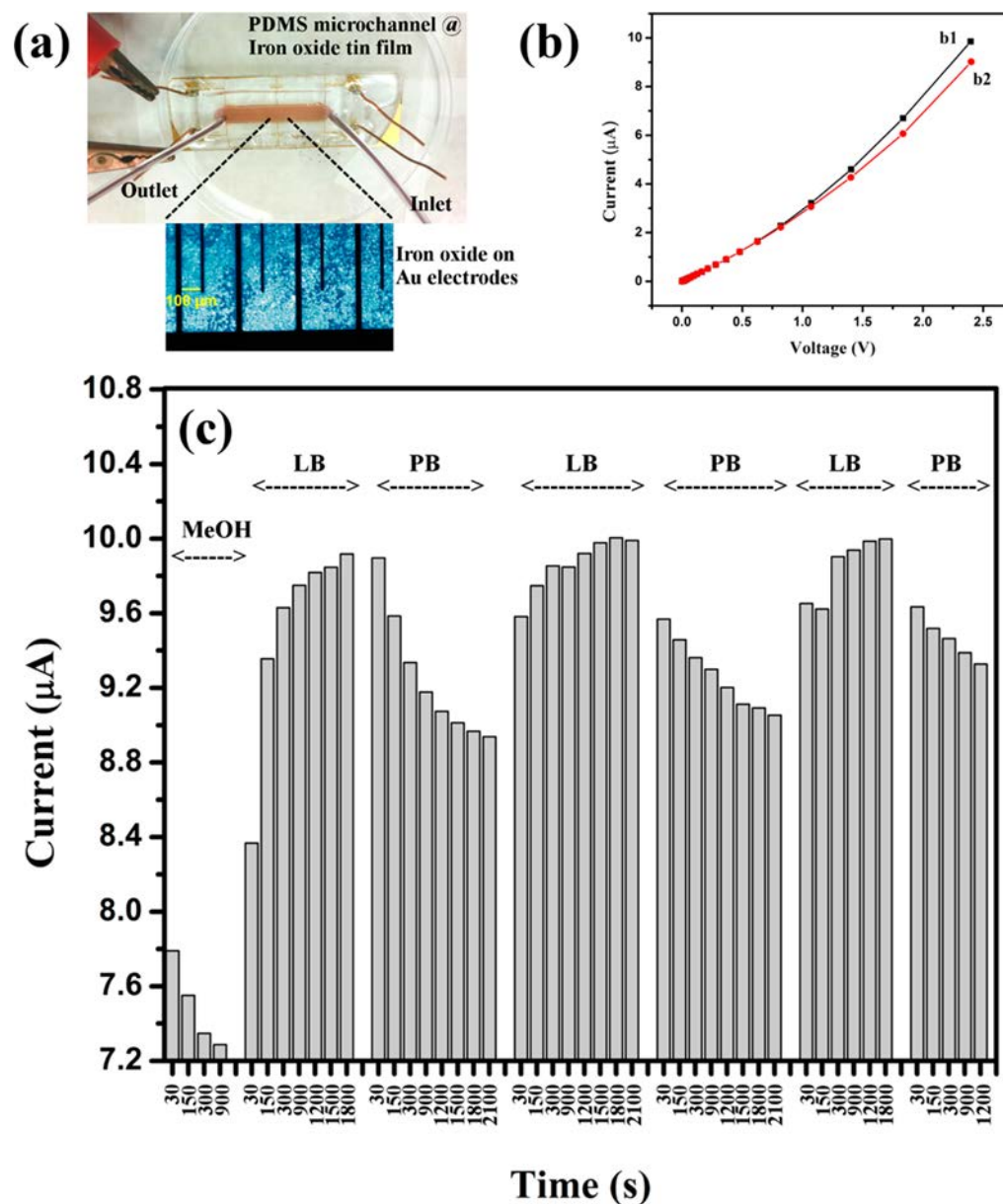


Figure 11. (a) Microfluidic channel fabricated on top of the 14.2 nm iron oxide-coated interdigitated gold electrodes. (b) Plot of current vs voltage of the iron oxide-coated gold electrode after 1500 s of flowing PCAT LB in MeOH (b1) and PCAT PB in MeOH (b2) into the microchannel. (c) Plot of current vs time by applying a bias voltage of 2.4 V to the iron oxide-coated gold electrodes while flowing MeOH, PCAT LB in MeOH, and PCAT PB in MeOH in the microchannel for three consecutive measurements.

change and makes the comparison between the intensity of the satellite and $2p_{3/2}$ peaks of each samples impossible.

Conductivity Measurement of Iron Oxide by a Microfluidic Device. An alternative path for better understanding the interaction of PCAT with iron oxide is through monitoring the change in conductivity of iron oxide while in contact with different oxidation states of PCAT (reduced and oxidized). Thus, we have fabricated a microfluidic device to sense these expected variations (Figure 11a). Because the thin fabricated iron oxide film (14.2 nm thick) has a high resistivity, we have used an array of closely packed interdigitated gold electrodes. Current–voltage curves were acquired by sweeping the bias logarithmically from 1 mV to 2.4 V in 5 min intervals while each analyte was flowing through the channel over the iron oxide film (flow rate = 0.2 mL/min). In the first run, pure MeOH was pushed through the channel. Subsequently, the

same measurement was repeated three times while PCAT LB and PCAT PB solutions (3 mg/mL in MeOH) were flowing through the channel. Figure 11b shows the I – V curves of the iron oxide film upon exposure to flows of PCAT LB and PCAT PB solutions. Both curves are nonlinear, which is characteristic of semiconducting materials. By flowing MeOH through the channel, the measured current starts to slowly decrease, indicating an increase in the electrical resistance of the iron oxide (Figure 11c). This indicates that the fabricated iron oxide film is not in its most oxidized form. However, when PCAT LB starts to flow, the current starts to increase quickly until reaching the stable value of $9.91 \mu\text{A}$ after 1800 s of exposure to this analyte. The trend reverses when flowing PCAT PB through the channel as the current starts to decrease to $8.99 \mu\text{A}$ after 2100 s of exposure.

This observation is in agreement with the results from our XPS, Raman spectroscopy, and previous reports,^{7,8} which suggest that upon adsorption of oxidized PCAT on iron oxide the organic molecules will be reduced by oxidizing the metal oxide substrate. This will lead to an increase in the electrical resistance of the iron oxide, and thus the current will decrease. On the other hand, the adsorption of reduced PCAT on iron oxide will result in the oxidation of PCAT and a slight reduction in the iron oxide, making it less electrically resistive. The reproducibility of this experiment was confirmed using a second fabricated device (Figure S18).

DISCUSSION

Although a majority of previous studies indicate that polyaniline coatings in their EB state are unable to protect steel against corrosion, some reports argue otherwise.^{8,59} PANI EB consists of 50% electron donor groups (secondary amines) and 50% electron acceptor groups (imines). It has previously been shown that half-oxidized PANI coatings are unable to induce a change in the polarity of the CNT substrate.⁶⁰ Despite the possibility of charge transfer to the substrate (e.g., native oxide on steel), because of its equal number of amine and imine groups the total net of the transferred charge at the interface is equal to zero. Therefore, a PANI EB coating is not able to change the potential of the underlying steel substrate and is not able to provide the overpotential necessary to form a passive iron oxide barrier layer. Our results showed that whereas an exact amount of oxidizing agent was employed for the preparation of PCAT EB, the result was not the half-oxidized state (Figure 1b). To the best of our knowledge, all of the synthesis routes for the preparation of PANI and its oligomers lead to the LB state.^{14,61,62} The lack of control over the chemical oxidation process during the preparation of the EB state leads to deviations from the structure consisting of exact 50% amine and 50% imine groups. Therefore, it is believed that the discrepancy in the results from the corrosion inhibition involving EB is related to the challenges associated with the preparation of the exact half-oxidized state of redox-active organic compounds. Our results indicate that under ambient conditions PCAT EB will be further oxidized on the surface of iron oxide (Figures 7a and 8a). This also provides another explanation for the previous reports on the ineffectiveness of EB in the corrosion inhibition of steel.^{63,64} Instead, we have shown that for the less-studied base state of redox-active oligoanilines, PB can withdraw electrons from the iron oxide substrate (Scheme 2f). All nitrogen atoms in the fully oxidized PCAT are in the sp^2 -hybridized imine form. Charge transfer from the steel substrate to the electron-accepting imine groups leads to the formation of a passive iron oxide film, whereas the PB film will be reduced to the lower oxidation states (Figure 7b). Because the base states of PCAT are not conductive, only the few first monolayers at the interface with the metal oxide will participate in the charge transfer. Therefore, a thin redox-active coating can be sufficient for the application in corrosion inhibition. Thus, to assess the success of a redox-active coating in corrosion inhibition, one has to consider the extent of charge transfer at the interface.

XPS has proven to be one of the most useful analytical tools for surface and interface studies. However, its limitation to the surface layers limits its use in studying the buried interfaces involved in the corrosion protection of metal/metal oxides by redox-active organic compounds. Most of the fabricated organic coatings used in previous studies are too thick for XPS to allow

access to the organic/oxide interface and have instead monitored the changes in the bulk of the top organic coatings.^{8,65} To avoid this issue, other reports have tried to study the metal oxide film instead by either chemically removing the organic coatings prior to the introduction of the sample to the XPS analysis chamber or by in situ sputtering.^{35,66} By removing the organic film, it was possible to study the surface of iron oxide surface, but it has been shown that sputtering of iron oxide can be destructive, causing the reduction of iron oxide.²² To tackle this issue, the organic coating was kept on the surface and instead the bare side of the steel substrate was analyzed by XPS.³⁴ However, because of the limitation of XPS to top surface layers, the measured data was only a representative of the bulk of the oxide layer and not the oxide surface in contact with the top organic coating. This is an important issue considering the layered structure of iron oxide.

We have demonstrated that oligoanilines such as PCAT are suitable redox-active compounds for studying the corrosion inhibition mechanism. PCAT has three oxidation state similar to those in PANI but can be deposited in a well-defined fashion via vacuum deposition. This provides the possibility for the fabrication of thin organic films, enabling the study of the top organic coating, the underlying metal oxide, and their interface at the same time (Figures 4, 6, and 7). In addition, the thin organic film minimizes bulk contributions to the inhibition process. XPS data on the interface between PB and iron oxide showed the expected reduction of the organic phase. In addition, it showed the appearance of charged nitrogen species. The appearance of these structures is associated with charge transfer at the interface. Under ambient conditions, the fully reduced PCAT coating on the iron oxide surface was quickly oxidized. Although the effect of ambient conditions in this oxidation process was previously suggested, we have observed the oxidization when the experiment was performed under high vacuum (Figure 6d). Even though the rate of oxidation was noticeably slower, it proved the contribution of the surface to this process. Although our XPS results showed that the changes in the organic coating fabricated on the metal oxide surface can be used as a gauge to indirectly monitor the changes in the underlying metal oxide, we were unable to observe such changes directly via XPS (Figure 10c). Therefore, we have used an alternative method to directly characterize these changes induced by a redox-active coating. For this purpose, changes in the resistivity of an ultrathin film of iron oxide through dynamic exposure to fully reduced and fully oxidized oligoanilines were monitored (Figure 11c). Even though this measurement is unable to provide any information about the structure of the iron oxide film, it has demonstrated the charge transfer at this interface. The resistivity of the iron oxide film during exposure to fully oxidized oligoaniline will increase because of the removal of defects (Fe^{2+}) from the iron oxide thin film via oxidation by oligoanilines. The reverse effect was observed while exposing the iron oxide thin film to the fully reduced oligoaniline. This process is associated with the oxidation of the organic film by the iron oxide at the expense of the reduction of the oxide film.

Charge transfer between organic thin films and metal oxide films (or other substrates) is of relevance not only in corrosion protection but also in organic electronics,^{3,5} sensor devices,^{67,68} and photocatalysis.^{69,70} Iron oxides (hematite in particular) have been studied for photocatalytic applications in water splitting for the hydrogen economy.^{69,71–73} The tuning of dopant levels plays an important role in preparing suitable

hematite photocatalysts,⁷⁴ but so far doping has been seen as a static, irreversible process. Here we have shown that the doping of iron oxide (hematite) films can be adjusted in situ via the redox state of adsorbed organic molecules. These molecules function to stabilize the iron oxide films and modulate their electronic structure (doping level, conductivity) reversibly. Although the label of interfacial doping has been applied to situations where the dopants were initially introduced at the interface and then allowed to diffuse into the bulk,⁷⁵ that scenario does not lend itself to switchable doping. What we demonstrate here is a modulation of the electronic structure of a semiconductor strictly through interfacial effects.⁷⁶ The electrochemical notion of a shift in corrosion potential^{1,7} is most compatible with the idea of redox potential doping (shift in band edge potentials regardless of charge-carrier transfer) rather than electronic doping.⁷⁷ Modifications to the band structure in the near-interface region (including but not limited to band bending) are commonly discussed in semiconductor physics,⁷⁶ but in nanoparticles and thin films, they can actually be considered to be a bulk phenomenon. Although indications of band structure modification (or maybe band bending) in the case of reduced PCAT on native iron oxide were found in an earlier study from our group,¹⁵ our results presented here are indicative of actual charge transfer, i.e., electronic doping, although we have not attempted to elucidate possible changes in the iron oxide band structure. Ways of distinguishing these different cases have been proposed,⁷⁷ but further work will be required on the PCAT/hematite system. Both doping mechanisms result in desirable changes in the electronic structure for electronic devices, sensors, and (photo)catalysts. Of particular interest are configurations where the doping level can be externally controlled. Electric field switchable devices (a.k.a. field-effect transistors, FETs) and photoswitchable devices, e.g., based on azo-benzenes,⁷⁸ are well-known, but we can now add redox-switchable dopants to our toolbox.

CONCLUSIONS

We have demonstrated the effect of iron oxide surfaces on redox-active PCAT molecules and vice versa. High-resolution XPS measurements have shown the partial reduction of fully and partially oxidized PCAT molecules at the interface with hematite (1000) single-crystal surfaces. Partial oxidation of fully reduced PCAT on an iron oxide surface has been reported for the first time. In situ deposition and XPS spectroscopy of the thin films of PCAT LB on steel have confirmed that this oxidation is truly mediated by the iron oxide substrate and not only by ambient conditions. These conclusions were confirmed through the use of Raman spectroscopy under ambient conditions. However, because of air oxidation, the degree of oxidation of PCAT LB is higher than what is observed in vacuum. This confirms the previous theory of the role of redox-active organic compounds in their oxidized states as oxidizers of the native iron oxide film.^{1,8} It also indicates the additional importance of air-exposed oxidation,¹⁹ in addition to the role of hematite in the completion of the redox cycle.

To understand why an organic molecule could experience both reduction and oxidation at the interface of a transition-metal oxide, it is important to consider that PCAT, in its base form, has three main oxidation states. It is known that PCAT, in its half-oxidized form, is in its most stable state. Although PCAT EB can be found in both asymmetrical and symmetrical isomers, in regard to their quinoid ring position it has been shown that the symmetrical form is thermodynamically more

stable than the asymmetrical form.^{79,80} This means that fully reduced PCAT (LB) at the interface with iron oxide (Fe^{2+} or Fe^{3+}) will be oxidized in order to reach the equilibrium half-oxidized state (EB). On the other hand, fully oxidized PCAT (PB) at the same interface will experience partial reduction in order to reach the half-oxidized state (EB).

We also showed that the conversion of PCAT base to its salt form by exposure to HCl does not lead to a considerable change in the oxidation states of PCAT but causes a drastic increase in the number of cationic nitrogen structures. It was also found that the PB and EB forms of PCAT can be doped approximately twice as much as the LB form through gas-phase protonic doping.

An important feature in the N 1s XPS spectra is the appearance of charged nitrogen structures in all oxidation states of PCAT at the interface with hematite. This is indicative of interfacial charge transfer between hematite and PCAT, which increases with the degree of oxidation of PCAT. Consistent with previous reports,^{32,33} this interfacial charge transfer can be considered to be a mutual interfacial doping process between the organic and the metal oxide phases. Further evidence for this interpretation comes from the possibility to detect the oxidation and reduction of ultrathin films of iron oxide using conductivity measurements on the iron oxide films.

Because of the close interactions of the redox states of both PCAT and iron oxide, modifications of the PCAT layer through acid–base or redox reactions can easily be detected through conductivity measurements. This can be utilized in the design of chemical sensing devices based on inexpensive iron oxide films. Molecular switches are an old concept, but practical examples of the facile detection of their state with a thin film sensor are less common. The facile doping and dedoping of iron oxide films in contact with different PCAT oxidation states is an example of interfacial doping with a switchable dopant, i.e., a molecular switch. The idea that a small local change in carrier concentration (in this case, due to a modification of the doping state) results in a large change in resistivity is somewhat reminiscent of (but not identical to) a chemical field-effect transistor (in which case the electric field is modulated by the creation of electric charges) in that it also constitutes an active sensor. In addition to applications in sensors, PCAT can also find use in the stabilization of iron oxide nanoparticles⁸¹ for biomedical applications, smart coatings (anticorrosion, controlled release),^{82,83} switchable membranes, and controlled adsorption.⁸⁴ PCAT and iron oxide form a fine-tuned system because of the alignment of the energy levels, but similar interactions could also apply to other surfaces if suitable ring substitutions for energy-level alignment are made. Although PCAT is a good model system by itself, polyaniline or other oligoanilines could be modified to also benefit from these interactions with iron oxide surfaces.

ASSOCIATED CONTENT

Supporting Information

The Supporting Information is available free of charge on the ACS Publications website at DOI: 10.1021/acs.jpcc.6b09950.

Additional data (mass spectrometry, UV–vis spectra, AFM, SEM, XPS spectra, and Raman spectroscopy) (PDF)

AUTHOR INFORMATION

Corresponding Author

*E-mail: pkruse@mcmaster.ca. Phone: (905) 525-9140 ext 23480. Fax: (905) 522-2509.

ORCID

Peter Kruse: 0000-0003-4051-4375

Notes

The authors declare no competing financial interest.

ACKNOWLEDGMENTS

We acknowledge technical assistance from and helpful discussions with P. Ravi Salvaganapathy, Andrew Broomfield, Steven A. Kornic, Kirk Green, James Britten, Jim Garrett, Leah Allan, Karen Neumann, Victoria Jarvis, and Enamul Hoque at McMaster University. Financial support was provided by the National Science and Engineering Research Council of Canada through the Discovery Grant program.

REFERENCES

- (1) Rohwerder, M. Conducting Polymers for Corrosion Protection: A Review. *Int. J. Mater. Res.* **2009**, *100*, 1331–1342.
- (2) Li, J.; Bao, Q.-Y.; Wei, H.-X.; Xu, Z.-Q.; Yang, J.-P.; Li, Y.-Q.; Lee, S.-T.; Tang, J.-X. Role of Transition Metal Oxides in the Charge Recombination Layer Used in Tandem Organic Photovoltaic Cells. *J. Mater. Chem.* **2012**, *22*, 6285–6290.
- (3) Kim, S. Y.; Baik, J. M.; Yu, H. K.; Lee, J.-L. Highly Efficient Organic Light-Emitting Diodes with Hole Injection Layer of Transition Metal Oxides. *J. Appl. Phys.* **2005**, *98*, 093707.
- (4) Chu, C.-W.; Li, S.-H.; Chen, C.-W.; Shrotriya, V.; Yang, Y. High-Performance Organic Thin-Film Transistors with Metal Oxide/Metal Bilayer Electrode. *Appl. Phys. Lett.* **2005**, *87*, 193508.
- (5) Greiner, M. T.; Helander, M. G.; Tang, W. M.; Wang, Z. B.; Qiu, J.; Lu, Z. H. Universal Energy-Level Alignment of Molecules on Metal Oxides. *Nat. Mater.* **2011**, *11*, 76–81.
- (6) DeBerry, D. W. Modification of the Electrochemical and Corrosion Behavior of Stainless Steels with an Electroactive Coating. *J. Electrochem. Soc.* **1985**, *132*, 1022–1026.
- (7) Wessling, B. Passivation of Metals by Coating with Polyaniline: Corrosion Potential Shift and Morphological Changes. *Adv. Mater.* **1994**, *6*, 226–228.
- (8) Beard, B. C.; Spellane, P. XPS Evidence of Redox Chemistry between Cold Rolled Steel and Polyaniline. *Chem. Mater.* **1997**, *9*, 1949–1953.
- (9) Rohwerder, M.; Isik-Uppenkamp, S.; Amarnath, C. A. Application of the Kelvin Probe Method for Screening the Interfacial Reactivity of Conducting Polymer Based Coatings for Corrosion Protection. *Electrochim. Acta* **2011**, *56*, 1889–1893.
- (10) Michalik, A.; Rohwerder, M. Conducting Polymers for Corrosion Protection: A Critical View. *Z. Phys. Chem.* **2005**, *219*, 1547–1559.
- (11) Wei, Y.; Jamasbi, H.; Cheng, S.; Jansen, S. A.; Sein, L. T.; Zhang, W.; Wang, C. Corrosion Protection Properties of Coating of the Epoxy-Cured Aniline Oligomers Based on Salt Spray and UV-Salt Fog Cyclic Tests. *ASC symp. Ser.* **2003**, *843*, 208–227.
- (12) Brown, B. P.; Picco, L.; Miles, M. J.; Faul, C. F. J. Conductive-AFM Patterning of Organic Semiconductors. *Small* **2015**, *11*, 5054–5058.
- (13) Zhang, W.; Yu, Y.; Chen, L.; Mao, H.; Wang, C.; Wei, Y. Synthesis and Study of Phenyl-Capped Tetraaniline as an Anti-corrosion Additive. *ACS Symp. Ser.* **2003**, *843*, 156–165.
- (14) Wang, W.; MacDiarmid, A. G. New Synthesis of Phenyl/phenyl End-Capped Tetraaniline in the Leucoemeraldine and Emeraldine Oxidation States. *Synth. Met.* **2002**, *129*, 199–205.
- (15) Greiner, M. T.; Festin, M.; Kruse, P. Investigation of Corrosion-Inhibiting Aniline Oligomer Thin Films on Iron Using Photoelectron Spectroscopy. *J. Phys. Chem. C* **2008**, *112*, 18991–19004.
- (16) Thomas, J. O.; Andrade, H. D.; Mills, B. M.; Fox, N. A.; Hoerber, H. J. K.; Faul, C. F. J. Imaging the Predicted Isomerism of Oligo(Aniline)s: A Scanning Tunneling Microscopy Study. *Small* **2015**, *11*, 3430–3434.
- (17) Kruger, J.; Yolken, H. T. Room Temperature Oxidation of Iron at Low Pressures. *Corrosion* **1964**, *20*, 29t–33t.
- (18) Kraljić, M.; Mandić, Z.; Duić, L. Inhibition of Steel Corrosion by Polyaniline Coatings. *Corros. Sci.* **2003**, *45*, 181–198.
- (19) Kinlen, P. J.; Silverman, D. C.; Jeffreys, C. R. Corrosion Protection Using Polyaniline Coating Formulations. *Synth. Met.* **1997**, *85*, 1327–1332.
- (20) Zhong, L.; Zhu, H.; Hu, J.; Xiao, S.; Gan, F. A Passivation Mechanism of Doped Polyaniline on 410 Stainless Steel in Deaerated H₂SO₄ Solution. *Electrochim. Acta* **2006**, *51*, 5494–5501.
- (21) Grosvenor, A. P.; Kobe, B. A.; McIntyre, N. S. Activation Energies for the Oxidation of Iron by Oxygen Gas and Water Vapour. *Surf. Sci.* **2005**, *574*, 317–321.
- (22) Biesinger, M. C.; Payne, B. P.; Grosvenor, A. P.; Lau, L. W. M.; Gerson, A. R.; Smart, R. S. C. Resolving Surface Chemical States in XPS Analysis of First Row Transition Metals, Oxides and Hydroxides: Cr, Mn, Fe, Co and Ni. *Appl. Surf. Sci.* **2011**, *257*, 2717–2730.
- (23) Fairley, N. CasaXPS, Revision 2.3.17; Casa Software Ltd: Teignmouth, Devon, U.K., 2016.
- (24) Moonosawmy, K. R.; Kruse, P. Ambiguity in the Characterization of Chemically Modified Single-Walled Carbon Nanotubes: A Raman and Ultraviolet-Visible-Near-Infrared Study. *J. Phys. Chem. C* **2009**, *113*, 5133–5140.
- (25) Nečas, D.; Klapetek, P. Gwyddion: An Open-Source Software for SPM Data Analysis. *Open Phys.* **2012**, *10*, 181–188.
- (26) Wang, Y.; Torres, J. A.; Stieg, A. Z.; Jiang, S.; Yeung, M. T.; Rubin, Y.; Chaudhuri, S.; Duan, X.; Kaner, R. B.; Al, W. E. T. Graphene-Assisted Solution Growth of Vertically Oriented Organic Semiconducting Single Crystals. *ACS Nano* **2015**, *9*, 9486–9496.
- (27) Poncet, M.; Corraze, B.; Quillard, S.; Wang, W.; MacDiarmid, A. G. Elaboration and Characterizations of Oligoaniline Thin Films. *Thin Solid Films* **2004**, *458*, 32–36.
- (28) Kang, E. T.; Neoh, K. G.; Tan, K. L. The Intrinsic Redox States in Polypyrrole and Polyaniline: A Comparative Study by XPS. *Surf. Interface Anal.* **1992**, *19*, 33–37.
- (29) Chen, Y.; Kang, E. T.; Neoh, K. G.; Lim, S. L.; Ma, Z. H.; Tan, K. L. Intrinsic Redox States of Polyaniline Studied by High-Resolution X-Ray Photoelectron Spectroscopy. *Colloid Polym. Sci.* **2001**, *279*, 73–76.
- (30) Heeger, A. J. Semiconducting and Metallic Polymers: The Fourth Generation of Polymeric Materials (Nobel Lecture). *Angew. Chem., Int. Ed.* **2001**, *40*, 2591–2611.
- (31) Yue, J.; Epstein, A. J. Xps Study of Self-Doped Conducting Polyaniline and Parent Systems. *Macromolecules* **1991**, *24*, 4441–4445.
- (32) Bai, S.; Zhao, Y.; Sun, J.; Tian, Y.; Luo, R.; Li, D.; Chen, A. Ultrasensitive Room Temperature NH₃ Sensor Based on Graphene-Polyaniline Hybrid Loading on PET Thin Film. *Chem. Commun.* **2015**, *51*, 7524–7527.
- (33) Xu, D.; Xu, Q.; Wang, K.; Chen, J.; Chen, Z. Fabrication of Free-Standing Hierarchical Carbon Nanofiber/graphene Oxide/polyaniline Films for Supercapacitors. *ACS Appl. Mater. Interfaces* **2014**, *6*, 200–209.
- (34) Fahlman, M.; Jasty, S.; Epstein, A. J. Corrosion Protection of Iron/Steel by Emeraldine Base Polyaniline: An X-Ray Photoelectron Spectroscopy Study. *Synth. Met.* **1997**, *85*, 1323–1326.
- (35) Talo, A.; Passiniemi, P.; Forsén, O.; Yläsaari, S. Polyaniline/Epoxy Coatings with Good Anti-Corrosion Properties. *Synth. Met.* **1997**, *85*, 1333–1334.
- (36) Zheng, W.; Angelopoulos, M.; Epstein, A. J.; MacDiarmid, A. G. Experimental Evidence for Hydrogen Bonding in Polyaniline: Mechanism of Aggregate Formation and Dependency on Oxidation State. *Macromolecules* **1997**, *30*, 2953–2955.
- (37) Jones, F.; Rohl, A. L.; Farrow, J. B.; van Bronswijk, W. Molecular Modeling of Water Adsorption on Hematite. *Phys. Chem. Chem. Phys.* **2000**, *2*, 3209–3216.

- (38) Leist, U.; Ranke, W.; Al-Shamery, K. Water Adsorption and Growth of Ice on Epitaxial $\text{Fe}_3\text{O}_4(111)$, $\text{FeO}(111)$ and $\text{Fe}_2\text{O}_3(\text{biphase})$. *Phys. Chem. Chem. Phys.* **2003**, *5*, 2435–2441.
- (39) Joseph, Y.; Ranke, W.; Weiss, W. Water on $\text{FeO}(111)$ and $\text{Fe}_3\text{O}_4(111)$: Adsorption Behavior on Different Surface Terminations. *J. Phys. Chem. B* **2000**, *104*, 3224–3236.
- (40) Baer, D. R.; Engelhard, M. H.; Lea, A. S. Introduction to Surface Spectroscopy Data on Electron and X-Ray Damage: Sample Degradation during XPS and AES Measurements. *Surf. Sci. Spectra* **2005**, *10*, 47–56.
- (41) Heister, K.; Zharnikov, M.; Grunze, M.; Johansson, L. S. O.; Ulman, A. Characterization of X-Ray Induced Damage in Alkanethiolate Monolayers by High-Resolution Photoelectron Spectroscopy. *Langmuir* **2001**, *17*, 8–11.
- (42) Kinlen, P. J.; Menon, V.; Ding, Y. A Mechanistic Investigation of Polyaniline Corrosion Protection Using the Scanning Reference Electrode Technique. *J. Electrochem. Soc.* **1999**, *146*, 3690–3695.
- (43) Heller, D. A.; Barone, P. W.; Swanson, J. P.; Mayrhofer, R. M.; Strano, M. S. Using Raman Spectroscopy to Elucidate the Aggregation State of Single-Walled Carbon Nanotubes Using Raman Spectroscopy to Elucidate the Aggregation State of Single-Walled Carbon Nanotubes. *J. Phys. Chem. B* **2004**, *108*, 6905–6909.
- (44) Boyer, M.-I.; Quillard, S.; Rebourt, E.; Louarn, G.; Buisson, J. P.; Monkman, A.; Lefrant, S. Vibrational Analysis of Polyaniline: A Model Compound Approach. *J. Phys. Chem. B* **1998**, *102*, 7382–7392.
- (45) Lindfors, T.; Kvarnström, C.; Ivaska, A. Raman and UV-Vis Spectroscopic Study of Polyaniline Membranes Containing a Bulky Cationic Additive. *J. Electroanal. Chem.* **2002**, *518*, 131–138.
- (46) Kinlen, P. J.; Ding, Y.; Silverman, D. G. Corrosion Protection of Mild Steel Using Sulfonic and Phosphonic Acid-Doped Polyanilines. *Corrosion* **2002**, *58*, 490–497.
- (47) Li, P.; Tan, T. C.; Lee, J. Corrosion Protection of Mild Steel by Electroactive Polyaniline Coatings. *Synth. Met.* **1997**, *88*, 237–242.
- (48) Sathiyarayanan, S.; Muthukrishnan, S.; Venkatachari, G.; Trivedi, D. C. Corrosion Protection of Steel by Polyaniline (PANI) Pigmented Paint Coating. *Prog. Org. Coat.* **2005**, *53*, 297–301.
- (49) Armelin, E.; Meneguzzi, A.; Ferreira, C. A.; Alemán, C. Polyaniline, Polypyrrole and poly(3,4-Ethylenedioxythiophene) as Additives of Organic Coatings to Prevent Corrosion. *Surf. Coat. Technol.* **2009**, *203*, 3763–3769.
- (50) Meroufel, A.; Deslouis, C.; Touzain, S. Electrochemical and Anticorrosion Performances of Zinc-Rich and Polyaniline Powder Coatings. *Electrochim. Acta* **2008**, *53*, 2331–2338.
- (51) Paliwoda-Porebska, G.; Rohwerder, M.; Stratmann, M.; Rammelt, U.; Duc, L. M.; Plieth, W. Release Mechanism of Electrodeposited Polypyrrole Doped with Corrosion Inhibitor Anions. *J. Solid State Electrochem.* **2006**, *10*, 730–736.
- (52) Holness, R. J.; Williams, G.; Worsley, D. A.; McMurray, H. N. Polyaniline Inhibition of Corrosion-Driven Organic Coating Cathodic Delamination on Iron. *J. Electrochem. Soc.* **2005**, *152*, B73–B81.
- (53) Aldissi, M.; Armes, S. P. X-Ray Photoelectron Spectroscopy Study of Bulk and Colloidal Polyaniline. *Macromolecules* **1992**, *25*, 2963–2968.
- (54) Xue, M.; Wang, S.; Wu, K.; Guo, J.; Guo, Q. Surface Structural Evolution in Iron Oxide Thin Films. *Langmuir* **2011**, *27*, 11–14.
- (55) Weiss, W.; Ranke, W. Surface Chemistry and Catalysis on Well-Defined Epitaxial Iron-Oxide Layers. *Prog. Surf. Sci.* **2002**, *70*, 1–151.
- (56) Evain, M.; Quillard, S.; Corraze, B.; Wang, W.; MacDiarmid, A. G. A Phenyl-End-Capped Tetramer of Aniline. *Acta Crystallogr., Sect. E: Struct. Rep. Online* **2002**, *58*, o343–o344.
- (57) Lemire, C.; Bertarione, S.; Zecchina, A.; Scarano, D.; Chaka, A.; Shaikhutdinov, S.; Freund, H. J. Ferryl ($\text{Fe}=\text{O}$) Termination of the Hematite $\alpha\text{-Fe}_2\text{O}_3(0001)$ Surface. *Phys. Rev. Lett.* **2005**, *94*, 166101.
- (58) Tang, Y.; Qin, H.; Wu, K.; Guo, Q.; Guo, J. The Reduction and Oxidation of $\text{Fe}_2\text{O}_3(0001)$ Surface Investigated by Scanning Tunneling Microscopy. *Surf. Sci.* **2013**, *609*, 67–72.
- (59) Spinks, G. M.; Dominis, A. J.; Wallace, G. G.; Tallman, D. E. Electroactive Conducting Polymers for Corrosion Control: Part 2. Ferrous Metals. *J. Solid State Electrochem.* **2002**, *6*, 85–100.
- (60) Klinke, C.; Chen, J.; Afzali, A.; Avouris, P. Charge Transfer Induced Polarity Switching in Carbon Nanotube Transistors. *Nano Lett.* **2005**, *5*, 555–558.
- (61) Sun, Z. C.; Jing, X. B.; Wang, X. H.; Li, J.; Wang, F. S. Synthesis and Characterisation of Phenyl-Capped Oligoanilines. *Synth. Met.* **2001**, *119*, 399–400.
- (62) Lu, F. L.; Wudl, F.; Nowak, M.; Heeger, A. J. Phenyl-Capped Octaaniline (COA): An Excellent Model for Polyaniline. *J. Am. Chem. Soc.* **1986**, *108*, 8311–8313.
- (63) Williams, G.; Gabriel, A.; Cook, A.; McMurray, H. N. Dopant Effects in Polyaniline Inhibition of Corrosion-Driven Organic Coating Cathodic Delamination on Iron. *J. Electrochem. Soc.* **2006**, *153*, B425–B433.
- (64) Gabriel, A.; Laycock, N. J.; McMurray, H. N.; Williams, G.; Cook, A. Oxidation States Exhibited by In-Coating Polyaniline during Corrosion-Driven Coating Delamination on Carbon Steel. *Electrochem. Solid-State Lett.* **2006**, *9*, B57–B60.
- (65) Affrossman, S.; Comrie, R. F.; MacDonald, S. M. Interaction of a Model Epoxy Resin Compound, Diethanolamine, with Aluminium Surfaces Studied by Static SIMS and XPS. *J. Chem. Soc., Faraday Trans.* **1998**, *94*, 289–294.
- (66) Virtanen, S.; Moser, E. M.; Böhni, H. XPS Studies on Passive Films on Amorphous Fe-Cr-(B,P)-C Alloys. *Corros. Sci.* **1994**, *36*, 373–384.
- (67) Capone, S.; Manera, M. G.; Taurino, A.; Siciliano, P.; Rella, R.; Luby, S.; Benkovicova, M.; Siffalovic, P.; Majkova, E. $\text{Fe}_3\text{O}_4/\gamma\text{-Fe}_2\text{O}_3$ Nanoparticle Multilayers Deposited by the Langmuir-Blodgett Technique for Gas Sensor Application. *Langmuir* **2014**, *30*, 1190–1197.
- (68) Hsu, L. H. H.; Hoque, E.; Kruse, P.; Ravi Selvaganapathy, P. A Carbon Nanotube Based Resettable Sensor for Measuring Free Chlorine in Drinking Water. *Appl. Phys. Lett.* **2015**, *106*, 063102.
- (69) Liu, Y.; Yu, Y.-X.; Zhang, W.-D. Photoelectrochemical Properties of Ni-Doped Fe_2O_3 Thin Films Prepared by Electrodeposition. *Electrochim. Acta* **2012**, *59*, 121–127.
- (70) Zhang, Y.; Cao, Y.; Wang, C.; Gao, J.; Xie, T.; Bai, Y. Study of Charge Transition Between Interfaces of Hetero-Structured Assemblies Based on Phenyl-Capped Aniline Tetramer/ $n(p)$ -Silicon. *J. Photochem. Photobiol., A* **2001**, *139*, 175–179.
- (71) Chatman, S.; Pearce, C. I.; Rosso, K. M. Charge Transport at Ti-Doped Hematite (001)/Aqueous Interfaces. *Chem. Mater.* **2015**, *27*, 1665–1673.
- (72) Toroker, M. C. Theoretical Insights into the Mechanism of Water Oxidation on Nonstoichiometric and Titanium-Doped $\text{Fe}_2\text{O}_3(0001)$. *J. Phys. Chem. C* **2014**, *118*, 23162–23167.
- (73) Kumar, P.; Sharma, P.; Shrivastava, R.; Dass, S.; Satsangi, V. R. Electrodeposited Zirconium-Doped $\alpha\text{-Fe}_2\text{O}_3$ Thin Film for Photoelectrochemical Water Splitting. *Int. J. Hydrogen Energy* **2011**, *36*, 2777–2784.
- (74) Liao, P.; Toroker, M. C.; Carter, E. A. Electron Transport in Pure and Doped Hematite. *Nano Lett.* **2011**, *11*, 1775–1781.
- (75) Ye, L.; Pujari, S. P.; Zuilhof, H.; Kudernac, T.; de Jong, M. P.; van der Wiel, W. G.; Huskens, J. Controlling the Dopant Dose in Silicon by Mixed-Monolayer Doping. *ACS Appl. Mater. Interfaces* **2015**, *7*, 3231–3236.
- (76) Cahen, D.; Kahn, A. Electron Energetics at Surfaces and Interfaces: Concepts and Experiments. *Adv. Mater.* **2003**, *15*, 271–277.
- (77) Schimpf, A. M.; Knowles, K. E.; Carroll, G. M.; Gamelin, D. R. Electronic Doping and Redox-Potential Tuning in Colloidal Semiconductor Nanocrystals. *Acc. Chem. Res.* **2015**, *48*, 1929–1937.
- (78) Basuki, S. W.; Schneider, V.; Strunskus, T.; Elbahri, M.; Faupel, F. Light-Controlled Conductance Switching in Azobenzene-Containing MWCNT-Polymer Nanocomposites. *ACS Appl. Mater. Interfaces* **2015**, *7*, 11257–11262.
- (79) Yanagida, S.; Manseki, K.; Segawa, H. Theoretical Evaluation of Electron Transport in Aniline Tetramer-Based Dye-Sensitized Solar Cells. *Electrochim. Acta* **2015**, *179*, 169–173.
- (80) Manseki, K.; Yu, Y.; Yanagida, S. A Phenyl-Capped Aniline Tetramer for Z907/*tert*-Butylpyridine-Based Dye-Sensitized Solar

Cells and Molecular Modelling of the Device. *Chem. Commun.* **2013**, 49, 1416–1418.

(81) Wei, W.; Wang, G.; Yang, S.; Feng, X.; Müllen, K. Efficient Coupling of Nanoparticles to Electrochemically Exploited Graphene. *J. Am. Chem. Soc.* **2015**, *137*, 5576–5581.

(82) Lv, L.; Zhao, Y.; Vilbrandt, N.; Gallei, M.; Vimalanandan, A.; Rohwerder, M.; Landfester, K.; Crespy, D. Redox Responsive Release of Hydrophobic Self-Healing Agents from Polyaniline Capsules. *J. Am. Chem. Soc.* **2013**, *135*, 14198–14205.

(83) Vimalanandan, A.; Lv, L.; Tran, T.; Landfester, K.; Crespy, D.; Rohwerder, M. Redox-Responsive Self-Healing for Corrosion Protection. *Adv. Mater.* **2013**, *25*, 6980–6984.

(84) Small, L. J.; Wheeler, D. R.; Spoerke, E. D. Nanoporous Membranes with Electrochemically Switchable, Chemically Stabilized Ionic Selectivity. *Nanoscale* **2015**, *7*, 16909–16920.